Estuarine, Coastal and Shelf Science 340 (2026) 109976

Contents lists available at ScienceDirect

Estuarine, Coastal and Shelf Science

journal homepage: www.elsevier.com/locate/ecss

Unveiling optical and phytoplankton variability in the northwestern Iberian Peninsula using in-situ radiometry and the Water Colour Simulator – WASI

Amália Maria Sacilotto Detoni [a,b,*,2], Natalia Rudorff Oliveira [c], Maria Laura Zoffoli [d], Peter Gege [e], Isabel Caballero [f], Gabriel Navarro [f], Marcos Fontela [b], María Jesús Álvarez Fernandéz [b], María López Serrano [b], Laura Moreno [b,g,1], Isabel Gomes Teixeira [b], Antón Velo [b], Xosé Antonio Padín [b,**]

[a] Nantes Université, Institut des Substances et Organismes de la Mer, ISOMER, UR 2160, Nantes, F-44000, France
[b] Instituto de Investigaciones Mariñas (IIM), Consejo Superior de Investigaciones Científicas (CSIC), Vigo, 36208, Spain
[c] Instituto Nacional de Pesquisas Espaciais (INPE), Dutra km 39, Cachoeira Paulista, SP, Brazil
[d] Consiglio Nazionale dele Ricerche, Istituto di Scienze Marine (CNR-ISMAR), Trieste, 34149, Italy
[e] Deutsches Zentrum für Luft- und Raumfahrt (DLR), Remote Sensing Technology Institute, Oberpfaffenhofen, Wessling, 82234, Germany
[f] Instituto de Ciencias Marinas de Andalucía (ICMAN), Consejo Superior de Investigaciones Científicas (CSIC), Campus Río San Pedro, Puerto Real, 11510, Spain
[g] CESAM – Centre for Environmental and Marine Studies and Department of Biology, University of Aveiro, Campus de Santiago, Aveiro, 3810-193, Portugal

ARTICLE INFO

Keywords:
Water-colour radiometry
Optical water types
Water-colour inversion
Optically active constituents
Phytoplankton composition
Rías baixas
Iberian upwelling system

ABSTRACT

The seasonal and spatial variability of optical and phytoplankton-related properties was investigated in Ría de Arousa and Ría de Vigo, two large embayments within the northwestern Iberian upwelling system. Over one year, quasi-monthly in-situ sampling was conducted to measure remote sensing reflectance (R_{rs}) alongside biophysical variables. Apparent and inherent optical properties (AOPs and IOPs, respectively), including absorption by phytoplankton, detritus, and coloured dissolved organic matter (CDOM), were analysed. Phytoplankton group composition (cyanobacteria, dinoflagellates, diatoms, cryptophytes, and green algae) and IOPs were retrieved using the *Water Colour Simulator* (WASI), applied to the R_{rs} dataset (380, 395, 412, 443, 465, 490, 510, 555, 670, 694, 710 nm). Model outputs were evaluated against in-situ chlorophyll-a concentrations (Chl-a), demonstrating satisfactory agreement. $R_{rs}(\lambda)$ spectra exhibited low reflectance in blue bands (<490 nm) associated with strong absorption by water constituents, and elevated reflectance in green-red bands (>490 nm), consistent with optically complex coastal waters. Phytoplankton was identified as the dominant optical constituent, followed by CDOM, whereas detritus showed the lowest absorption at 443 nm. Ría de Vigo was characterised by greater variability in R_{rs} and Chl-a, likely reflecting its more confined hydrodynamics and enhanced local retention processes. Seasonal shifts were observed with increased microplankton contribution during summer in Ría de Arousa and higher variability in phytoplankton size structure in Ría de Vigo. These findings highlight the capability of WASI to resolve bio-optical variability and community dynamics in estuarine waters, supporting its application for aquaculture management and ecosystem monitoring in optically complex coastal systems.

1. Introduction

Water colour radiometry has produced vast datasets that drive the development of high-quality water colour products for a range of biogeochemical applications and water quality monitoring (Xi et al., 2017; Bi et al., 2023). Central to these advancements are physically based models, which enable, through inverse modelling, quantitative retrieval of inherent optical properties (IOPs) that describe the

* Corresponding author. Nantes Université, Institut des Substances et Organismes de la Mer, ISOMER, UR 2160, F-44000, Nantes, France.
** Corresponding author.
E-mail addresses: amaliadetoni@gmail.com (A.M.S. Detoni), padin@iim.csic.es (X.A. Padín).
[1] CESAM – Centre for Environmental and Marine Studies and Department of Biology, University of Aveiro, Campus de Santiago, Aveiro, 3810-193, Portugal (current address).
[2] Nantes Université, Institut des Substances et Organismes de la Mer, ISOMER, UR 2160, F-44000 Nantes, France (current address).

https://doi.org/10.1016/j.ecss.2026.109976
Received 25 September 2025; Received in revised form 11 May 2026; Accepted 13 May 2026
Available online 23 May 2026

absorption and scattering characteristics of seawater constituents and have provided significant advances in this field (IOCCG, 2006; Werdell et al., 2014). Nonetheless, despite its potential, the accuracy of inverse modelling is often challenged by spectral ambiguities of the reflectance spectrum of water and the limitations of the satellite data, such as the limited spatial and spectral resolution, uncertainties in atmospheric correction, and sensor noise (IOCCG, 2006; Sun et al., 2025). Consequently, validation against in-situ measurements is critical to ensure their accuracy and applicability across varying aquatic environments (Xi et al., 2017). Concurrently, in-situ radiometry has evolved as an alternative tool to assess and monitor water quality, particularly for coastal and inland systems (Niroumand-Jadidi et al., 2021; Bi et al., 2023; Maire et al., 2025). Besides enabling the inversion of IOPs and biogeochemical constituents, the reflectance spectrum can be used to classify aquatic environments into Optical Water Types (OWT), which share similarities in their IOPs and dominant constituents. This approach is also emerging as a robust tool to monitor these systems, characterizing their optical properties and the associated uncertainties of each class for optical and biogeochemical inversion. Ultimately, OWT classification schemes have been used to select more appropriate optical models and/or parametrization to improve water colour inversion for each type (Wei et al., 2022).

Ría de Vigo and Ría de Arousa are two important shellfish aquaculture areas of the Rías Baixas, which comprises four elongated coastal embayments in Galicia, northwestern (NW) Spain, near the northern border of the Iberian upwelling ecosystem (Fig. 1A and B). In southern Rías Baixas, a long-term monitoring time series (1994-2020) indicated that potentially toxic blooms of the dinoflagellate *Alexandrium minutum* are recurrent and may be increasing in extent and intensity, as well as exhibiting regional expansion (Nogueira et al., 2022; Rodríguez et al., 2024). These recurrent Harmful Algal Blooms (HABs) represent a growing concern due to their negative impacts on the aquaculture sector, including prolonged shellfish harvesting closures (Detoni et al., 2024). In this context, changing climate conditions have been suggested to contribute to the observed increase in HAB occurrences, especially in the NW Iberian Peninsula shelf over recent decades (Álvarez-Salgado et al., 2008; Rodríguez et al., 2024), highlighting the need for sustained monitoring efforts.

Ocean-colour remote sensing in coastal waters enables the optical characterization of seawater and the retrieval of key constituents, including chlorophyll-a concentration (Chl-a), a proxy for phytoplankton biomass, as well as the light absorption of coloured dissolved organic matter (CDOM) and detrital material (non-algal suspended matter) (Werdell et al., 2014). Additionally, it offers the potential to identify dominant phytoplankton groups from multi- and hyperspectral ocean colour data. The *Water Colour Simulator* - WASI is a radiative transfer inversion tool designed for the modelling and analysis of optical in-situ remote sensing reflectance (R_{rs}) spectra (Gege, 2004). It enables the simulation and retrieval of bio-optical properties in aquatic environments using several well-established analytical models. Here, the remote sensing reflectance model of Albert (Albert and Mobley, 2003; Albert, 2004) is used. The variability of the R_{rs} spectrum is controlled by up to 25 parameters, depending on the spectrum type and environmental characteristics of the water body (Albert and Mobley, 2003). The model estimates the absorption spectra of the optically active constituents (OACs), *i.e.,* phytoplankton, detritus, and CDOM, allowing them to vary independently. Additionally, WASI enables the differentiation of phytoplankton functional groups (cyanobacteria, dinoflagellates, diatoms, cryptophytes, and green algae) through the application of analytical models that assign distinct specific absorption spectra and corresponding fractionated Chl-a to distinct optical classes. This capability makes WASI a valuable tool for investigating the optical properties of optically complex aquatic systems and assessing phytoplankton community composition.

With the increasing availability of operational ocean-colour satellite sensors and advancements in sensor resolutions and atmospheric correction algorithms, more accurate satellite estimates of water-leaving radiance and R_{rs} are becoming more achievable. However, the reliable inversion of these signals to derive IOPs and OAC concentrations remains a challenge, particularly in optically complex coastal waters. The Rías Baixas present additional challenges due to their narrow geometry and complex coastal configuration. Current satellite sensors remain constrained either by spatial, temporal, or spectral resolution, limiting their capacity to resolve these systems. Therefore, in-situ radiometry remains an essential approach to characterize and monitor these systems and validate satellite observations.

Based on the first radiometric campaigns collected across Ría de Arousa and Ría de Vigo on the NW Iberian coast, the present study aims to characterize the optical water types and variability of the IOPs and phytoplankton community structure of these systems, using in-situ radiometry and the WASI inversion framework. This study provides new insights into the spatiotemporal variation of ocean-colour properties in these estuaries, which are of significant socioeconomic and ecological importance and are increasingly affected by climate change (Rodríguez et al., 2024).

2. Materials and methods

2.1. Study area and in-situ sampling

The Rías Baixas are a system of V-shaped coastal embayments located along the southern coast of Galicia (NW Spain). This study focuses on two estuaries (Arousa and Vigo, Fig. 1B), which are connected to the North Atlantic Ocean and receive freshwater inputs from rivers discharging into their inner sectors. The Ría de Vigo is influenced by freshwater input from the River Verdugo, which exhibits marked seasonal variability, with higher discharge during winter and reduced flow in summer. It has a maximum depth of approximately 53 m at the outer southern entrance, a surface area of about 176 km^2, and a length of ~21 km (Barton et al., 2015). The Ría de Arousa, the largest of the Rías Baixas, is primarily fed by the River Ulla, characterised by a comparable seasonal discharge regime, reaching peak flows in winter. It has a maximum depth of 69 m at its mouth, a total surface area of 239 km^2, and spans a length of 33 km (Pardo et al., 2022).

Sampling was conducted at approximately monthly frequency over one year (September 2023–October 2024), yielding a total of 72 collections of biogeochemical, physical, and radiometric parameters, within the surface layer and at depths with vertical radiometric and CTD profiles. Of these, 33 collections were obtained at five stations in Ría de Arousa, and 39 at three regular stations in Ría de Vigo, with an additional opportunistic collection obtained once at a fourth station (V6). This sampling design ensured good spatial and temporal coverage within each estuary, allowing the characterisation of the variability in environmental, optical, and biological parameters.

2.2. In-situ radiometry

Spectral in-water downwelling irradiance ($E_d(\lambda)$) and upwelling radiance ($L_w(\lambda)$) were measured at 11 wavebands (380, 395, 412, 443, 465, 490, 510, 555, 670, 694, and 710 nm; bandwidth of 10 nm) using a profiling reflectance radiometer (PRR-800; Biospherical Instruments®), following protocol recommendations of the International Ocean Colour Coordinating Group (Zibordi et al., 2019). After applying standard calibration and pre-processing routines (including dark spectrum and lamp calibration), the PRR-800 was deployed at the downwind side of the starboard, letting the instrument drift away enough to avoid shadow from the vessel before profiling (Zibordi et al., 2019). The instrument was deployed twice at each station, for duplicate measurements.

The diffuse attenuation coefficients for $E_d(\lambda)$ ($k_d(\lambda)$) and $L_u(\lambda)$ ($k_u(\lambda)$) were determined following Smith and Baker (1986), as the local slope of ln $[E_d(z, \lambda)]$ and ln $[L_u(z, \lambda)]$ using a linear regression fit, assuming constant values along the water column within a selected depth interval

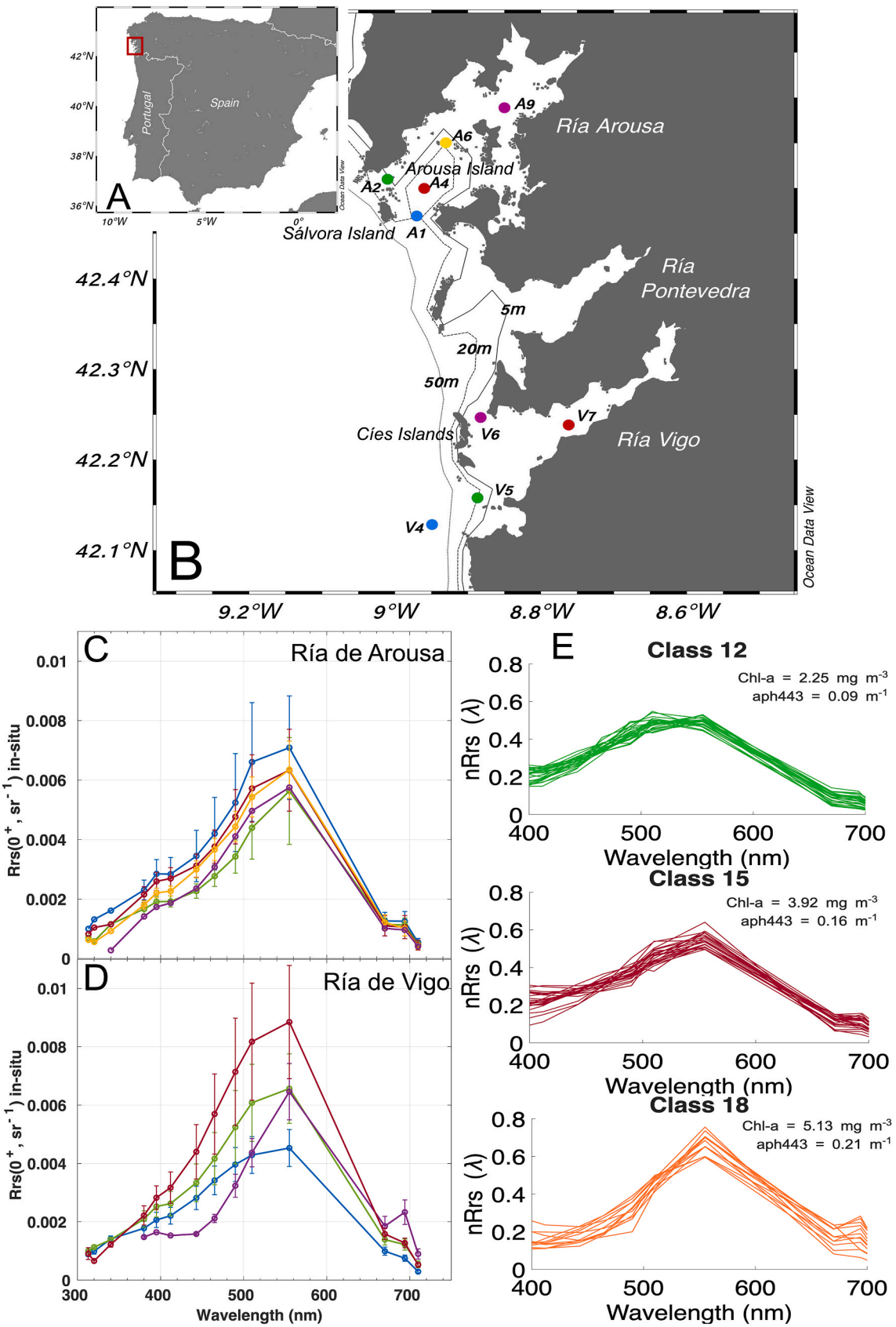

Fig. 1. (A) The Iberian Peninsula, with the red rectangle indicating the sampling embayments shown in panel (B). (B) Study area with the in-situ collection stations. "A" stands for Ría de Arousa and "V" for Ría de Vigo, the sequential numbers correspond to their relative positioning from the open ocean, and the colour-codes correspond to the annual mean ($R_{rs}(0^+,\lambda)$) measured at each station and shown in (C) and (D). (E) Normalized in-situ $R_{rs}(\lambda)$ ($nR_{rs}(\lambda)$) spectra classified according to Wei et al. (2022), showing for each water type the median in-situ Chl-a (measured by fluorimetry) and median phytoplankton absorption coefficient estimated by WASI (aph443). (For interpretation of the references to colour in this figure legend, the reader is referred to the Web version of this article.)

(~11 m). This interval was chosen according to a visual inspection of each $E_d(\lambda)$ and $L_u(\lambda)$ profile, selecting the interval closest to the surface and with the least noise.

The above water-leaving radiance (L_w, 0^+) was then determined using the extrapolated $L_u(z)$ to just below the surface (L_u, 0^-, Eq. (1)) and the water-air transmittance factor (Eq. (2)), as follows:

$$L_u(0^-,\lambda) = L_u(z,\lambda)\cdot\exp\,(k_u \cdot z) \tag{1}$$

$$L_w(0^+,\lambda) = L_u(0^-,\lambda)\cdot 0.543 \tag{2}$$

The water downwelling irradiance ($E_d(0^+,\lambda)$ was determined using the extrapolated Ed(z) to just below the surface ($E_d(0^-,\lambda)$ (Eq. (3)) accounting for the loss due to the upward air–water interface reflection and gain of the downward reflected flux (Eq. (4)):

$$E_d(0^-,\lambda) = E_d(z,\lambda)\cdot\exp\,(k_d \cdot z) \tag{3}$$

$$E_d(0^+,\lambda) = E_d(0^-,\lambda)\cdot\frac{\left(1 - r\cdot\left(\frac{L_u(0^-,\lambda)\,\cdot\,3.14}{E_d(0^-,\lambda)}\right)\right)}{(1-\rho)} \tag{4}$$

where r is the mean water-air Fresnel reflectance factor for the diffuse upward flux ($r \cong 0.48$) and ρ is the bulk air-water Fresnel reflectance factor for the downward irradiance of the Sun and sky reflected on the surface ($\rho \cong 0.32$) (Morel and Antoine, 1994).

The remote sensing reflectance just above the water surface ($(R_{rs}(0^+,\lambda)$), defined as the ratio between $L_w(0^+,\lambda)$ and $E_d(0^+,\lambda)$, was finally obtained at each spectral band of the PRR-800 (Eq. (5)).

$$R_{rs}(0^+,\lambda) = \frac{L_w(0^+,\lambda)}{E_d(0^+,\lambda)} \tag{5}$$

2.3. Physical and biogeochemical properties

Temperature, salinity, and pressure were obtained from downcast profiles collected using a conductivity-temperature-depth (CTD) sensor (Sea-Bird SBE 25plus), and were used to compute the potential density of seawater and the mixed-layer depth (MLD) using the finite difference criteria method (modified from Glover and Brewer (1988) and Kara et al. (2000)). Seawater samples were collected with Niskin bottles mounted on the CTD frame at approximately 2 m and at the depth of the phytoplankton fluorescence maximum for Chl-a determination using the fluorometric method (Neveux and Panouse, 1987). The reported Chl-a values correspond to the average concentration between surface and fluorescence maximum depths (ranging from 10 to 25 m).

Additionally, surface water samples for High-Performance Liquid Chromatography (HPLC) pigments analysis (Zapata et al., 2000) were collected at station V7 (inner region of the Ría de Vigo) during separate cruises within ±2 days of the radiometric sampling, with the same frequency (quasi-monthly) over the year-round period. Although this temporal offset may introduce variability in phytoplankton composition, meteorological and hydrographic conditions remained comparable during both sampling days, allowing these measurements to provide complementary characterization of the dominant phytoplankton groups at this station. Pigment composition was obtained using the Pigmentum software (Bilbao and Seoane, 2024), which classifies phytoplankton groups based on diagnostic pigments and their relative contribution to total Chl-a, covering picoplankton (cell size: 0.2–2 μm), nanoplankton (cell size: 2–20 μm), and microplankton (cell size: 20–200 μm).

Microscopic optical identification and cell count of microphytoplankton (cell size: 20–200 μm), including dinoflagellates and diatoms, were also analysed at each station, within surface water samples. The samples were preserved with Lugol's iodine in 100 mL Pyrex bottles and stored in the dark until analysis. Cell enumeration was conducted using an inverted microscope at 100× magnification, following the Utermöhl (1958) sedimentation method with 10-50 mL settling chambers, depending on the Chl-a previously measured for coincident collections. Cell counts were converted to cellular carbon biomass ($\mu gC\cdot L^{-1}$) using Menden-Deuer and Lessard (2000), based on biovolumes calculated according to Hillebrand et al. (1999). Subsequently, carbon-to-chlorophyll-a (C:Chl-a) ratios were applied to the microscopy-based carbon estimates for dinoflagellates and diatoms, using conversion factors of 60 $mgC\cdot mg^{-1}$Chl-a and 40 $mgC\cdot mg^{-1}$Chl-a, respectively, as proposed by Sathyendranath et al. (2009).

2.4. Inversion of the optical water constituents and phytoplankton groups

The absorption coefficients of phytoplankton (a_{phy}), detritus (a_{det}), and CDOM (a_{CDOM}) were retrieved through inverse modelling of $R_{rs}(0^+,\lambda)$ measurements using WASI (Gege, 2004). The inversion scheme relies on a non-linear optimization using the Downhill Simplex algorithm (Nelder and Mead, 1965; Gege and Albert, 2006). Within the WASI inversion framework, $a_{phy}(\lambda)$ is represented as a combination of up to six predefined phytoplankton groups: cyanobacteria, dinoflagellates, diatoms, cryptophytes, green algae, and a mixed phytoplankton component (hereafter referred to as non-identified phytoplankton, NI) (Eq. (6); Gege, 2004). As no species-specific phytoplankton absorption spectra for the study area were available, specific absorption spectra $a_i^*(\lambda)$ from the WASI database were taken. Cyanobacteria (phycoerythrin-dominant) $a_i^*(\lambda)$ was obtained from field measurements in the Baltic Sea during cyanobacterial blooms, likely dominated by *Nodularia* sp. (Xi et al., 2017). Cryptophyte $a_i^*(\lambda)$ was derived from field measurements of cryptophyte-dominant assemblages, characterised by a pronounced absorption peak at 550 nm and a strong correlation with alloxanthin concentration. $a_i^*(\lambda)$ representing dinoflagellates, diatoms, and green algae were obtained from laboratory-grown reference cultures (*Gymnodinium breve*, *Asterionella formosa*, and *Chlorella vulgaris*, respectively) included in the WASI database. $a_i^*(\lambda)$ of the NI class was derived from hundreds of field measurements representing an average mixture of different phytoplankton species, mainly cryptophytes, diatoms, and dinoflagellates. With the known $a_i^*(\lambda)$, inverse modelling retrieves the group-specific Chl-a (C_i). When phytoplankton can be represented by a single $a_i^*(\lambda)$, the remaining C_i terms are constrained to zero, following the standard WASI configuration (Gege, 2004).

$$a_{phy}(\lambda) = \sum_{i=1}^{6} C_i \cdot a_i^{*}(\lambda) \tag{6}$$

Total Chl-a was calculated as the sum of the retrieved C_i's (Eq. (7)):

$$Chl\text{-}a = \sum_{i=1}^{6} C_i \tag{7}$$

To validate the group-specific C_i, only dinoflagellates and diatoms were quantified by microscopy analysis for all stations. Alternatively, HPLC measurements available only for station V7 were used to analyse the inversion retrievals of the other groups. Given that the WASI inversion relies on predefined a_{phy} classes, the retrieved phytoplankton groups were interpreted within a size-based ecological framework. In this interpretation, cyanobacteria and chlorophyll-b-containing phytoplankton (green algae optical class) were associated with the picoplankton fraction, cryptophytes with nanoplankton, and dinoflagellates and diatoms with microplankton, and an additional category for NI taxa. This size-based classification is a widely used ecological framework that links phytoplankton community structure to physiology, nutrient uptake, trophic interactions, and carbon cycling (Marañón, 2015; Uitz et al., 2006).

In addition, for comparison, we estimated total Chl-a from in-situ $R_{rs}(0^+,\lambda)$ using the empirical global 3-band Ocean Colour algorithm (OC3, O'Reilly and Werdell, 2019), and the Quasi-Analytic Algorithm (QAA, Lee et al., 2002, Lee, 2014). The OC3 algorithm is based on three spectral bands at 443, 490, and 560 nm (Eq. (8)), and it was developed for Case-1 waters, *i.e.*, where CDOM and phytoplankton concentrations co-vary. The polynomial coefficients (O'Reilly and Werdell, 2019) are

given for the PRR-800 sensor bands based on the OC3 maximum band ratio ($\frac{R_{rs}(\lambda b)}{R_{rs}(\lambda g)}$), *i.e.,* $R_{rs}(443 > 490)/R_{rs}(555)$. $a_0 = 0.3308$; $a_1 = -2.6684$; $a_2 = 1.5990$; $a_3 = 0.5525$; $a_4 = -1.4876$.

$$\log_{10}(Chl-a) = a_0 + a_1X + a_2X^2 + a_3X^3 + a_4X^4, X = \log_{10}\frac{R_{rs}(\lambda b)}{R_{rs}(\lambda g)} \quad (8)$$

The IOP inversion-based QAA algorithm (Lee et al., 2002, Lee, 2014) is commonly adopted for ocean and coastal water applications. The algorithm separates the total absorption coefficient into contributions from pure water absorption ($a_w(\lambda)$), $a_{phy}(\lambda)$, and combined CDOM plus detritus absorption ($a_{dg}(\lambda)$). To estimate Chl-a from $a_{phy}(\lambda)$ (Eq. (9)) we used a global average value for $a^*_{phy}(443) = 0.0448$ $m^2 \cdot mg^{-1}$ (Maritorena et al., 2002).

$$Chl\text{-}a = \frac{a_{phy}(443)}{a^*_{phy}(443)} \quad (9)$$

2.5. Data analysis

For the optical characterization of the estuaries, we used the Optical Water Types (OWT) approach following Wei et al. (2022). First, the $R_{rs}(0+, \lambda)$ spectra were normalized and then classified into 23 possible OWTs using the endmembers provided by Wei et al. (2022) and a cosine distance (d) criterion (Eq. (10)), whereby the assigned OWT corresponded to the smallest d to the reference.

$$d = 1 - \frac{\sum_{i=1}^{5}[nR_{rs}(\lambda_i) \times R_{rs}(\lambda_i)]}{\sqrt{\sum_{i=1}^{5}[nR_{rs}(\lambda_i)]^2 \times \sum_{i=1}^{5}[R_{rs}\lambda_i]^2}} \quad (10)$$

where λ_1-λ_5 corresponds to the five Visible Infrared Imaging Radiometer Suite (VIIRS) spectral bands (410, 443, 486, 551, and 671 nm), while for the PRR-800 sensor, the corresponding 412, 443, 490, 555, and 670 nm bands were used. These classifications were used, along with the measured Chl-a and physical properties, to assess water quality and analyse the spatio-temporal variability of the estuaries.

Chl-a retrieved by WASI, OC3, and QAA was compared to the measured Chl-a using standard statistical metrics, *i.e.,* Coefficient of Determination (R^2), p-value, Root Mean Square Error (RMSE), Median Absolute Error (MedAE), bias (BIAS), and Unbiased Absolute Percentage Difference (UAPD). After the model evaluation, the spatio-temporal variability of the modelled IOPs and phytoplankton groups (C_i) was analysed, complementing the analysis of the measured properties of $R_{rs}(\lambda)$, Chl-a, sea surface temperature (SST), and MLD.

3. Results

3.1. Spatio-temporal variability of the measured optical, biogeochemical, and physical properties

The mean spectral magnitude and shape of the $R_{rs}(0^+, \lambda)$ of both estuaries are characteristic of optically complex coastal waters with a strong contribution from absorbing particulate and dissolved coloured substances. This is indicated by the lower $R_{rs}(0^+, \lambda)$ at the "blue" bands (<490 nm) associated with increased absorption, and higher $R_{rs}(0^+, \lambda)$ at the green bands (510 – 555 nm), indicative of enhanced backscattering of algal and detritus suspended particles. The higher R_{rs} peak at the Chl-a fluorescence band (694 nm) also indicated the presence of high phytoplankton biomass within these systems. The normalized $R_{rs}(0^+, \lambda)$ spectra in both *rías* were assigned to three optical classes: 12 (n = 27), 15 (n = 19), and 18 (n = 10) (Fig. 1E). These OWTs are characterized by "moderate (12) to turbid (15 and 18)" coastal waters with mixed contributions of phytoplankton, detritus and CDOM, influenced by continental sources. The measured Chl-a and estimated (WASI) absorption coefficient had approximate median values compared to those obtained by Wei et al. (2022) for each class (Table S1). These parameters will be briefly described to characterize the OWTs and discussed in more detail in the following sections.

The waters classified as OWT 12, are those defined as "moderately turbid coastal waters", with low R_{rs} at the shorter bands (<490 nm) and maximum peaks at the green bands (510 – 555 nm) (Fig. 1E). The median Chl-a was 2.25 mg m^{-3} (ranging from 0.84 to 5.04 mg m^{-3}) and $a_{CDOM}(443)$ was 0.07 m^{-1}. Phytoplankton contributed 45% to the biogenic absorption (at 443 nm) and CDOM 35% (on average). The waters classified as OWT 15 represented "turbid coastal waters" with a sharper decrease of R_{rs} at the blue bands (<490 nm) and a more pronounced R_{rs} peak at the longer green band (555 nm). The median Chl-a was somewhat higher, with 3.92 mg m^{-3} (ranging from 1.18 to 6.71 mg m^{-3}), as well as $a_{CDOM}(443)$ with 0.13 m^{-1}. Phytoplankton contributed 50% of the biogenic absorption (at 443 nm) and CDOM 41%. Finally, the waters classified as OWT 18 corresponded to "turbid coastal waters", with increased phytoplankton biomass. This class showed significantly lower R_{rs} at the shorter blue bands (<510 nm) and at the red Chl-a absorption band (670 nm), alongside a more pronounced R_{rs} peak at the longer green band (555 nm) and Chl-a fluorescence band (694 nm), indicative of higher phytoplankton concentration. This OWT had the highest median Chl-a (5.13 mg m^{-3}, ranging from 2.74 to 14.68 mg m^{-3}) and $a_{CDOM}(443)$ (0.18 m^{-1}) (Fig. 1E and Table S1). The contributions of phytoplankton and CDOM to the biogenic absorption were similar to OWT 12 (with 49% and 42%, respectively). For the three OWTs, phytoplankton and CDOM were the primary contributors shaping the R_{rs} spectra and defining the water types. $a_{det}(443)$, on the other hand, had approximately the same median for the three OWTs (0.03 – 0.04 m^{-1}), with a relatively low contribution to the bulk biogenic absorption, especially for OWTs 15 and 18 (9% compared to 20% for OWT 12) (Fig. 1 and Table S1).

No clear spatial or temporal patterns were observed in the classification of the OWTs across both Ría de Arousa and Ría de Vigo, but some finer variability observed for the R_{rs} is described as follows.

The annual mean $R_{rs}(\lambda)$ in Ría de Arousa exhibited relatively low spectral variability within the estuary, compared to Ría de Vigo, with overall higher magnitudes observed at stations located from the mid-estuary towards the outer region, particularly through the deep southern mouth (~70 m) (Fig. 1D). Lower $R_{rs}(\lambda)$ magnitudes were recorded at the innermost station (A9) and at station A2, located near Sálvora Island at the northern mouth, where a shallow channel (~10 m depth) connects the estuary to the open ocean. $R_{rs}(\lambda)$ at 490 – 555 nm, also exhibited a relatively high annual standard deviation, especially for the mid-outer stations, denoting a significant variability throughout the year in these more dynamic areas.

In Ría de Vigo, greater variability in both the magnitude and spectral shape of $R_{rs}(\lambda)$ was observed across stations compared to Ría de Arousa (Fig. 1E). Over the annual sampling period, a gradient from higher to lower $R_{rs}(\lambda)$ magnitudes was observed from the inner estuary towards open ocean waters. Only two radiometric profiles were collected at the northern mouth of the estuary (station V6; August 7 and September 5, 2024). They showed a distinct spectral signature, with lower $R_{rs}(\lambda)$ at shorter wavelengths (<490 nm) and a pronounced peak at the Chl-a fluorescence band (694 nm), indicating higher phytoplankton concentrations typical of late-summer conditions. $R_{rs}(\lambda)$ at 490 – 555 nm also exhibited high standard deviation, especially for the inner (V7) and southern mouth (V5) stations, suggesting seasonal or sporadic episodes of increased contributions of absorbing and scattering constituents (Fig. 1E).

In summary, both estuaries showed $R_{rs}(\lambda)$ primarily shaped by a higher presence of blue-band absorbing constituents, especially phytoplankton and CDOM, compared to more open ocean waters (V4), with lower $R_{rs}(\lambda)$ at the blue bands, and higher $R_{rs}(\lambda)$ at the green (*e.g.,* 555 nm) and red Chl-a fluorescence (694 nm) bands. Regardless of spatial location or sampling period, the *rías* were thus classified as Case-2 waters belonging to OWTs 12, 15, and 18 according to Wei et al. (2022). The main differences between the two estuaries were that, in

addition to the lower $R_{rs}(\lambda)$ spectral variability observed in Ría de Arousa, the station with the highest $R_{rs}(\lambda)$ values in the green-red bands was located at the southern deep mouth (A1). In contrast, in the Ría de Vigo, the highest green-red $R_{rs}(\lambda)$ values were observed in the innermost area (V7), located in the mid estuary. These differences likely reflect contrasting coastal dynamics between the two systems (Figueiras and Pazos, 1991; Álvarez-Salgado et al., 2008). The outer region of the Ría de Arousa, characterized by a wider and more open configuration, is strongly influenced by coastal upwelling and oceanic water intrusions, which enhance phytoplankton productivity and optical variability near the mouth of the estuary. In contrast, the Ría de Vigo, which is narrower and more elongated, is more influenced by inner estuarine processes. Its geomorphological configuration favours stronger stratification and a well-defined two-layer estuarine circulation, with seaward transport in the surface layer and landward intrusion of saline water at depth. In addition, river discharge, particle resuspension in shallow areas, and longer water residence times (Álvarez-Salgado et al., 2008) may enhance suspended matter and phytoplankton biomass toward the inner sector. Together, these processes contribute to the observed spatial differences in $R_{rs}(\lambda)$ and highlight the role of contrasting coastal dynamics in shaping the optical properties of both systems.

During winter, spring, and autumn, the sea surface temperature (SST) and MLD exhibited similar ranges in both estuaries, with SST between approximately 14 and 16 °C and MLD between about 10 and 15 m. The largest seasonal differences were observed during summer. In the Ría de Arousa, SST exhibited a horizontal gradient, with lower values (~15 °C) in the outer sector, which is more influenced by coastal upwelling, and higher values (~17 °C) in the inner and shallower sector. During the same period, the MLD in the Ría de Arousa was generally shallower (<15m). In contrast, SST in Ría de Vigo was more homogeneous along the embayment (~16 °C), and MLD was deeper (>15 m) during summer (Fig. 2).

Mean in-situ Chl-a over the sampling period was very similar in Ría de Arousa (4.00 mg m^{-3}) and Ría de Vigo (4.12 mg m^{-3}). However, greater spatio-temporal variability was observed in Ría de Vigo (standard deviation of 3.23 mg m^{-3}) compared to Ría de Arousa (±1.52 mg m^{-3}), consistent with the higher variability observed in $R_{rs}(\lambda)$. Seasonal and spatial variability of the Chl-a is further analysed in the following section, along with the retrieved IOPs and phytoplankton groups.

3.2. Modelled optical and biogeochemical properties

Among the three tested methods to retrieve Chl-a from $R_{rs}(\lambda)$, the results derived from WASI exhibited the best overall performance, with R^2 of 0.49 and the lowest MedAE (0.74 mg m^{-3}), systematic bias (0.41 mg m^{-3}), and UAPD (25.5%) (Fig. 3). These results indicate good agreement between WASI retrievals and in-situ Chl-a measurements, supporting its applicability in optically complex coastal waters. In contrast, the OC3 algorithm showed the lowest performance, with the lowest R^2 (0.36) and the highest RMSE (17.29 mg m^{-3}), MedAE (1.7 mg m^{-3}), and UAPD (53%) (Fig. 3), indicating greater deviations from observed Chl-a values and limited suitability for this study area. The QAA algorithm, which is suitable for complex coastal waters, showed performance comparable to that of WASI and improved over OC3. However, it underestimated Chl-a by 1.02 mg m^{-3}, and its overall performance remained slightly inferior to that of WASI (R^2 = 0.49, RMSE = 2.42 mg m^{-3}, MedAE = 1.62 mg m^{-3}, and UAPD = 53.3%). The application of the WASI inversion to in-situ $R_{rs}(\lambda)$ measurements provided consistent estimates of Chl-a in both estuaries. Performance metrics were higher in Ría de Arousa, where optical conditions were more homogeneous (R^2 = 0.65, RMSE = 1.13 mg m^{-3}, MedAE = 0.74 mg m^{-3}, BIAS = 0.48 mg m^{-3}, and UAPD = 20%). In comparison, lower performance was obtained for Ría de Vigo (R^2 = 0.47, RMSE = 3.28 mg m^{-3}, MedAE = 0.77 mg m^{-3}, BIAS = 0.34 mg m^{-3}, and UAPD = 34.7%).

For the retrieved absorption coefficients, a higher mean $a_{phy}(443)$ was found in both estuaries (Fig. 4A, 0.171 ± 0.004 m^{-1} for Ría de Arousa and 0.172 ± 0.025 m^{-1} for Ría de Vigo; Table 1), suggesting dominance of phytoplankton over other OACs. Phytoplankton was the main contributor to the bulk biogenic absorption at 443 nm ($a_{bio}(443)$, defined by the sum of phytoplankton, CDOM and detritus absorption coefficients) at stations with elevated Chl-a, except for one offshore station (V4), where despite relatively high Chl-a (~1.0 mg m^{-3}), absorption was dominated by CDOM (~80%), likely indicating a senescent bloom stage (Fig. 4B). CDOM was the second most dominant OAC in both estuaries with intermediate mean $a_{CDOM}(443)$ (0.12 ± 0.03 m^{-1} for Ría de Arousa and 0.14 ± 0.02 m^{-1} for Ría de Vigo; Table 1). At most stations, $a_{bio}(443)$ was dominated by either phytoplankton or CDOM (Fig. 4B). Detritus consistently showed the lowest annual average absorption coefficients in both the Vigo and Arousa *rías* (0.04 ± 0.004 m^{-1} and 0.03 ± 0.02 m^{-1}, respectively) (Fig. 4A). Its contribution to the bulk $a_{bio}(443)$ exceeded 40% in only four cases: A1-late summer (outer southern station; Sep 12, 2023), V5-spring (outer southern station; Apr 18, 2024), and V7-winter and spring (mid-estuarine station; Jan 12 and Apr 19, 2024) (Fig. 4B). In-situ Chl-a measurements (obtained at A1, V5, and V7-winter) were relatively low in these cases (<1.6 mg·m^{-3}). For the case of station V7-spring, measured Chl-a was not available, but the retrieved (WASI) Chl-a was also relatively low (0.32 mg·m^{-3}).

The Chl-a associated with microplankton (C_m) (i.e., the combined

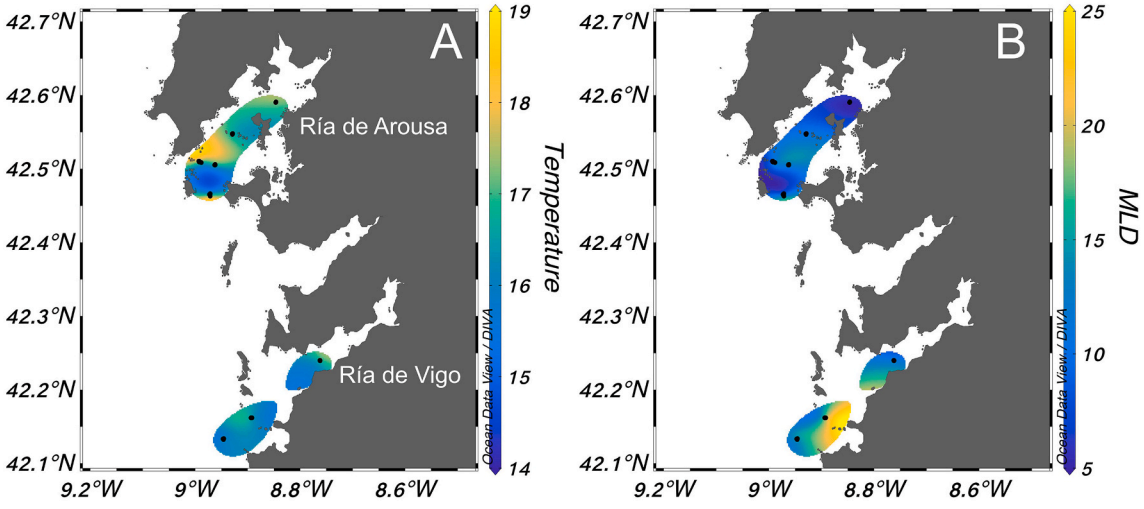

Fig. 2. The average surface distribution of (A) the sea surface temperature and (B) mixed layer depth (MLD). of the Ría de Arousa and Ría de Vigo.

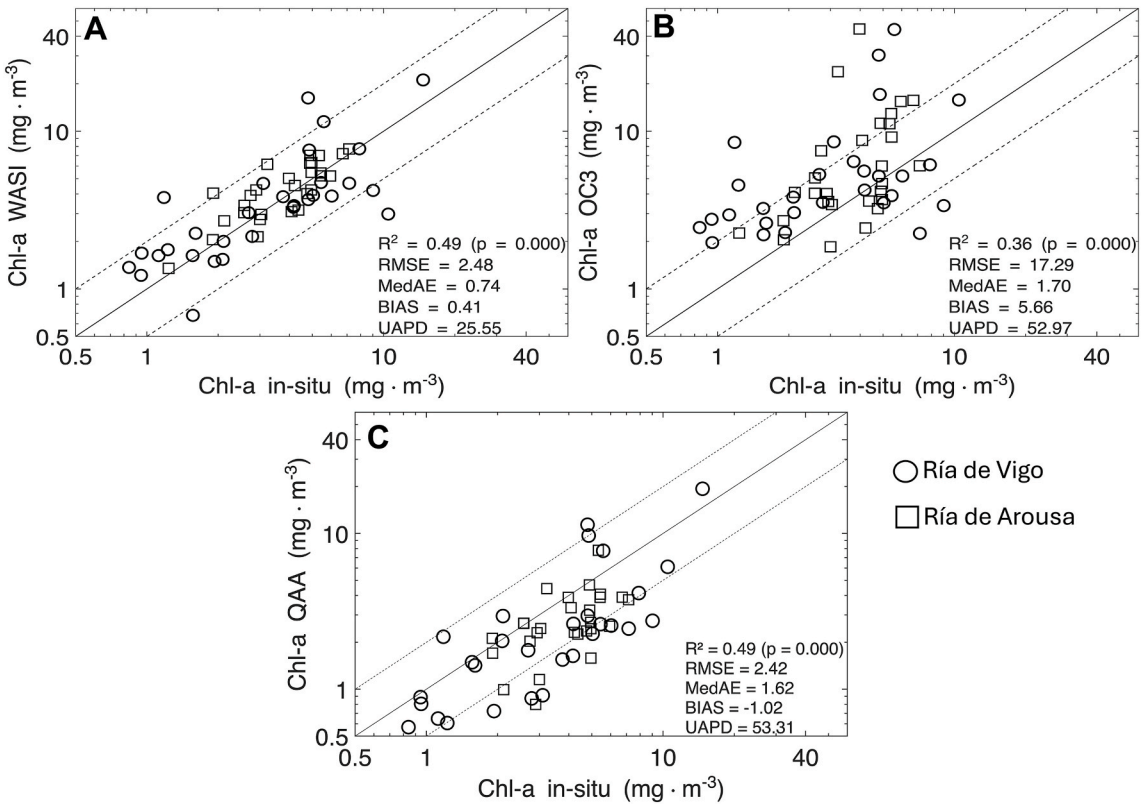

Fig. 3. Correlation between the in-situ Chl-a and Chl-a retrieved by (A) WASI, (B) OC3, and (C) QAA. Black lines correspond to 1:1 lines in all graphics, and dashed lines are the 1:2 and 2:1 lines.

contribution of dinoflagellates and diatoms) estimated by WASI showed a significant positive correlation with HPLC diagnostic pigment measurements (Fig. 5A) ($R^2 = 0.38$, $p = 0.019$). The regression slope of 0.74 indicates a slight underestimation relative to in-situ values, although the relationship remained linear across the observed range. Conversely, no significant correlation was found between WASI-derived and HPLC-based Chl-a for picoplankton (C_p) (*i.e.*, cyanobacteria and green algae) ($R^2 = 0.01$; $p = 0.77$), indicating limited skill in resolving this size class under the observed conditions (Fig. 5B). A significant positive correlation was also found between WASI-derived and microscopy-based C_m across both *rías* ($R^2 = 0.34$, $p = 0.001$). The slope of 0.50 and intercept of 0.14 suggest that WASI tended to underestimate higher in-situ values (Fig. 5C). Overall, these results indicate that WASI provides a reasonable estimate of microplankton biomass, while its performance for picoplankton, including cyanobacteria and green algae, remains limited under the prevailing optical conditions.

Both observed and inversion-derived Chl-a in Ría de Arousa (Fig. 6) and Ría de Vigo (Fig. 7) followed a clear seasonal pattern, with minimum levels recorded during winter (December 2023 to February 2024) and maxima between June and September 2024. These seasonal maxima coincide with the regional upwelling season (April to September), during which nutrient-rich water input typically triggers significant peaks in phytoplankton biomass (Detoni et al., 2024). While the seasonal variability of Chl-a was slightly lower in Ría de Arousa, in both estuaries phytoplankton community composition showed shifts during high-Chl-a events, such as the bloom observed in early June 2024 (Fig. 6). In this study, picoplankton refers to the combined contribution of cyanobacteria and green algae, whereas microplankton encompasses dinoflagellates and diatoms. These groups were the most frequently co-occurring assemblages throughout the study period. However, microplankton contributed most significantly during spring and early summer blooms, consistent with the typical successional sequence in the *rías* where diatoms and dinoflagellates dominate high-biomass events or "red-tides". In contrast, autumn and winter (November 2023 to February 2024) were characterized by lower phytoplankton diversity with a relative dominance of nano- and picoplankton (Fig. 6A–D and 7A, B, and D).

In Ría de Vigo (stations V4–V7), both in-situ and modelled Chl-a presented higher seasonal variability. Picoplankton and microplankton followed a similar pattern, with increased contributions during Chl-a peaks, particularly during late summer (August–October 2024). However, the relative contributions of NI, cryptophytes, pico- and microphytoplankton were more variable, indicating potential differences in nutrient availability or hydrodynamic conditions compared to Ría de Arousa. The differences in phytoplankton community structure between the two estuaries suggest distinct seasonal dynamics and might illustrate the different timing of the transition from microplankton-dominated upwelling phases to smaller-sized assemblages typically associated with more stable or downwelling-influenced conditions during winter in the Galician *rías*.

4. Discussion

The remote sensing of aquatic systems relies on a comprehensive understanding of IOPs, their variability, and their influence on water-colour radiometry. In this study, both AOPs and IOPs were used to characterize the optical properties and their spatio-temporal variability in the *rías* de Arousa and Vigo (NW Iberian coast), along with the succession of phytoplankton assemblages derived from ocean-colour inversion. Previous studies have demonstrated that $R_{rs}(\lambda)$ data, through inverse modelling of a physically based model, can effectively differentiate phytoplankton taxonomic groups (Gege, 1998; Werdell et al., 2014; Xi et al., 2017; Maire et al., 2025). Building on this framework, the WASI inversion was applied to in-situ $R_{rs}(\lambda)$ measurements to retrieve optical water constituents and phytoplankton community structure in the Ría de Arousa and Ría de Vigo, offering new

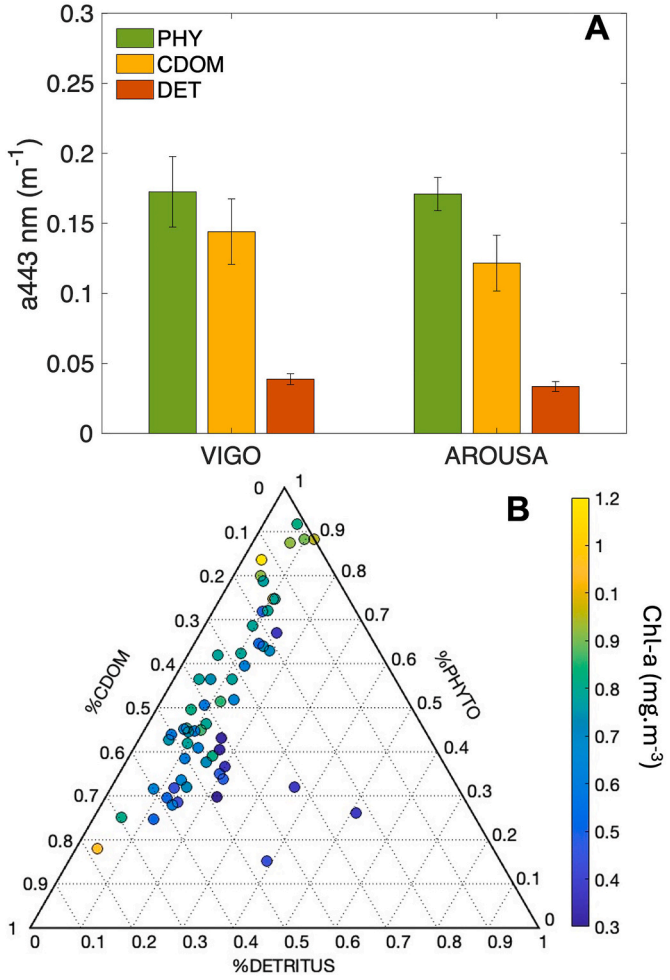

Fig. 4. (A) Mean absorption coefficients at 443 nm (a_{443}) for phytoplankton (PHY), coloured dissolved organic matter (CDOM), and detritus (DET) in the Ría de Vigo and Ría de Arousa. Error bars represent standard deviations. (B) Ternary diagram showing the relative contribution of CDOM (%CDOM), detritus (%DET), and phytoplankton (%PHY) to the total biogenic absorption at 443 nm in Ría de Vigo and Ría de Arousa. Points are colour-coded by the corresponding in-situ chlorophyll-a concentration (Chl-a, mg·m^{-3}). (For interpretation of the references to colour in this figure legend, the reader is referred to the Web version of this article.)

insights into their ecological dynamics. Results of the WASI inversion model exhibited good agreement with in-situ measurements despite the high optical complexity and variability within the study area (Fig. 1C, D, 1E, and 3). In addition, performance was improved relative to both the empirical OC3 and QAA algorithms (Fig. 3), consistent with previous studies in optically complex waters that demonstrated higher accuracy of the WASI inversion scheme over two other methods, including the OC3 and Case-2 Regional/Coast Colour (C2RCC) (Niroumand-Jadidi et al., 2021). A key advantage of WASI lies in its flexible inversion parametrization, which allows adaptation to diverse optical conditions and improves the retrieval of IOPs in dynamic aquatic environments. However, it should be noted that no region-specific IOPs were available, hence the inversion made use of predefined optical classes and specific absorption spectra, which may not fully capture the local phytoplankton composition and variability. In particular, the specific absorption spectra of cyanobacteria are highly variable due to substantial variation in intracellular pigment concentrations. Therefore, cyanobacteria spectrum used may not represent well the actual conditions at all stations, which may be a major reason for the low correlation of the picoplankton group (cyanobacteria + green algae) in Fig. 5B.

Following the classification scheme proposed by Wei et al. (2022), optical conditions in both the *rías* de Arousa and Vigo were predominantly assigned to three OWTs (Classes 12, 15, and 18). These classes span a gradient from moderately turbid coastal waters (Class 12) to increasingly turbid, more productive and optically complex environments (Classes 15 and 18). The ranges of in-situ Chl-a and inversion-derived IOPs observed in this study are consistent with global ranges reported by Wei et al. (2022) for these classes, supporting the representativeness of these classes for the Rías Baixas. However, their occurrence showed no consistent spatial or temporal pattern, instead reflecting local environmental variability. This variability is likely driven by seasonal forcing, including PAR availability, coastal upwelling, and river discharge, all of which have been shown to modulate the biophysical conditions and phytoplankton dynamics in these systems (Detoni et al., 2024). WASI inversion results indicate that phytoplankton and CDOM dominate absorption in both estuaries, whereas detritus remained mostly with a low contribution. These systems are influenced by several hydrodynamics and biophysical conditions including intense coastal upwelling events in the period from April to September (Pardo et al., 2011) driven by northerly winds, tidal cycles, prevailing winds, sea-atmosphere interactions, river discharge and sediment resuspension (Rosón et al., 1995, 1997). Besides the natural coastal dynamics influencing the optical properties of these estuaries, there is also a large number of mussel rafts contributing to CDOM and detritus accumulation in both *rías*. Nonetheless, there is a relatively high hydrodynamic connectivity of these systems with the open ocean, and the constant exchange seems to prevent massive accumulation of detrital matter, comprising non-living organic materials, within the estuarine systems (at least in the surface layer). Hence, phytoplankton was identified as the dominant optical constituent in both *rías*, with CDOM as the secondary contributor, also highlighting a major role of primary production and covarying organic matter release defining the optical characteristics of these coastal environments (Fig. 4A).

Table 1
Minimum, maximum, average, and standard deviation values at Ría de Arousa and Ría de Vigo of WASI parameters, microscopy, and in-situ Chl-a.

	Ría de Arousa				Ría de Vigo			
	Min	Max	Mean	Sd	Min	Max	Mean	Sd
Dino + Diato + Crypto (MICROSCOPY) (mg • m-3 Chl-a)	0.51	7.24	3.49	3.65	0.06	16.68	1.76	0.60
Dino + Diato + Crypto (WASI) (mg • m-3 Chl-a)	0.00	6.04	2.04	2.52	0.00	4.72	1.03	0.22
Cyano + Greeen (WASI) (mg • m-3 Chl-a)	0.00	21.13	2.97	5.68	0.00	13.87	2.28	0.51
Rrs(443) (sr-1)	0.001	0.009	0.003	0.000	0.001	0.014	0.003	0.000
Rrs(555) (sr-1)	0.003	0.017	0.006	0.000	0.002	0.028	0.007	0.000
Temp (°C)	13.78	18.24	15.37	0.76	13.44	18.48	15.21	0.24
MLD (m)	3.40	26.00	11.55	0.26	3.50	35.63	13.55	1.18
Chl-a situ (mg • m-3)	1.23	7.15	4.00	0.00	0.84	14.68	4.12	0.52
Chl-a wasi (mg • m-3)	1.35	7.71	4.60	0.56	0.32	21.13	4.46	0.70
aphy(443) (m-1)	0.048	0.312	0.171	0.004	0.012	0.758	0.172	0.025
acdom(443) (m-1)	0.006	0.558	0.122	0.027	0.000	0.617	0.144	0.023
adet(443) (m-1)	0.011	0.087	0.033	0.025	0.011	0.124	0.039	0.004

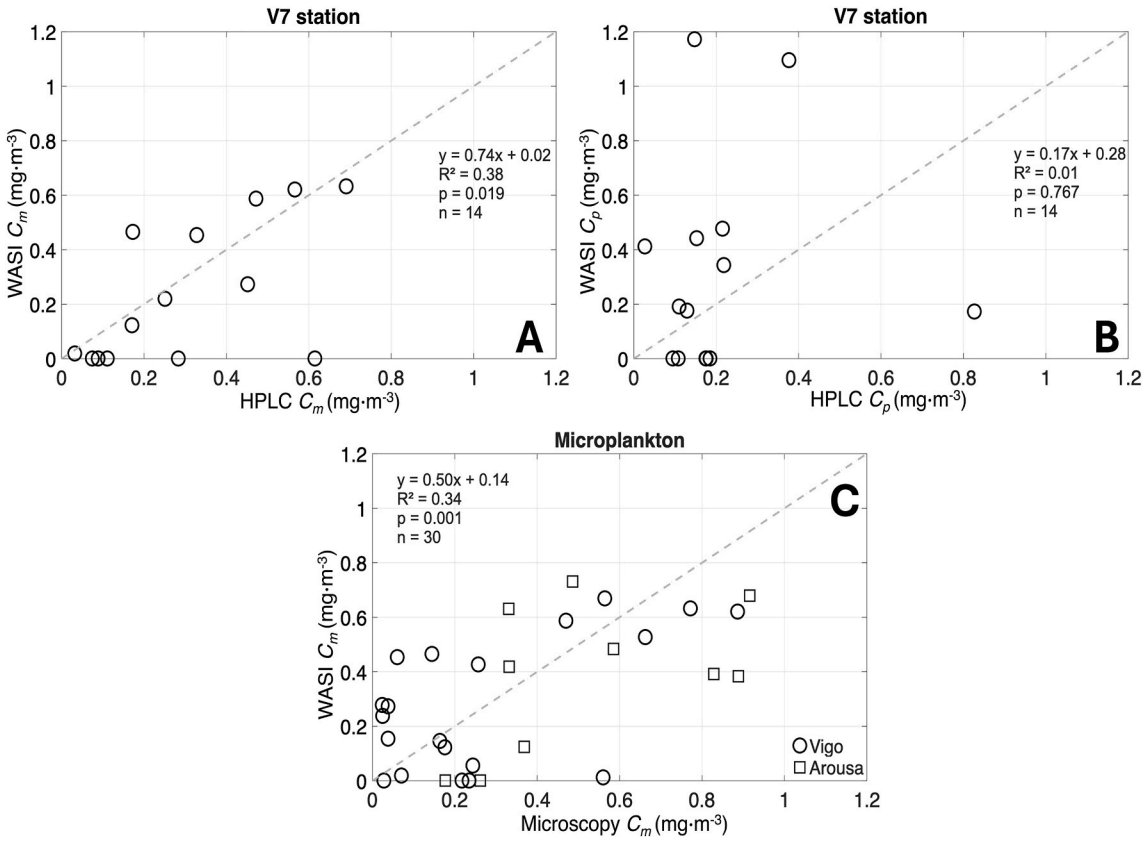

Fig. 5. Correlations between WASI-derived and observed Chl-a for microplankton (dinoflagellate + diatom) (C_m) (A, C) and picoplankton (cyanobacteria + green algae) (C_p) (B). Panels A–B show HPLC-based estimates of C_m and C_p from quasi-monthly measurements at station V7 (Ría de Vigo); panel C shows microscopy-based C_m across all stations in Ría de Vigo (circles) and Ría de Arousa (squares).

In terms of the spatio-temporal variability of the optical properties and Chl-a, these exhibited comparatively lower variability in the Ría de Arousa (mean: 4 ± 1.52 mg m^{-3}), partly reflecting the smaller sampling effort (8 campaigns versus 14 in Ría de Vigo). Despite this limitation, differences between the optical and biogeochemical properties of these two estuaries are consistent with their contrasting hydrodynamic regimes. The optical variability within Ría de Arousa was lower, with small flagellates dominating throughout the year and sharing dominance with microplankton in summer and picoplankton in winter. This is likely linked to this estuary's wider and more open morphology, together with the larger freshwater input from the Ulla River, which enhances water exchange and promotes more homogeneous hydrographic conditions. In contrast, the spatial and temporal variability of optical and biogeochemical properties within Ría de Vigo was greater, and the phytoplankton community composition was more heterogeneous, with contributions from micro-, nano-, and picoplankton. This pattern is consistent with its narrower, more elongated morphology, deeper MLD (particularly in summer under the influence of coastal upwelling), stronger two-layer estuarine circulation, and enhanced sediment resuspension.

The physical differences between the estuaries are reflected in the phytoplankton assemblages and succession. In the Ría de Vigo, a greater dominance of larger phytoplankton cells was generally observed, particularly during summer months marked by intense coastal upwelling (Rosón et al., 1995; Barton et al., 2015) and coincident with the peak of phytoplankton bloom activity. In the Ría de Arousa, where the MLD remained shallower, small flagellates tended to dominate throughout the year. These patterns are consistent with previous studies in the Rías Baixas, which highlighted the strong influence of hydrography on phytoplankton structure. Figueiras and Pazos (1991) reported that microplankton assemblages in Ría de Vigo were associated with subsurface Chl-a maxima and deeper MLD, whereas smaller flagellates dominated in Ría de Arousa under shallower MLD and regenerated nutrient conditions. Tilstone et al. (1994) described the role of upwelling-downwelling sequences in driving blooms of larger phytoplankton in Ría de Vigo. More recently, Figueiras et al. (2020) emphasized how nutrient traps in semi-enclosed bays control seasonal variability in microbial plankton communities.

Anthropogenic influences, particularly mussel aquaculture, may further modulate these dynamics. Froján et al. (2014) demonstrated that mussel farming in Ría de Vigo exerts top-down control by grazing on micro- and nanoplankton, reducing Chl-a and shifting the size structure of the microbial plankton, while picoplankton is largely unaffected. At the same time, regenerated nutrients from mussel excretion can stimulate phytoplankton growth in areas escaping grazing. In Ría de Vigo, this effect is linked to its 474 rafts (Organización de Productores de Mejillón de Galicia (OPMEGA), https://www.opmega.com), suggesting an even stronger influence in Ría de Arousa, where its 2319 rafts are present (Organización de Productores de Mejillón de Galicia (OPMEGA), https://www.opmega.com), further contributing to the observed differences in the phytoplankton assemblages and size structure. The Ría de Arousa, the largest of the Galician *rías*, has a wide and open configuration, with multiple islands (*e.g.,* Arousa Island and Sálvora Island) influencing internal circulation and a greater horizontal gradient of SST. Besides the top-down control of its extensive mussel production, the geomorphology of the Arousa estuary facilitates the exchange with oceanic waters and enhances water renewal and circulation, preventing excessive retention of detrital matter and promoting a more stable phytoplankton community. In contrast, the Ría de Vigo, with its narrower morphology, elongated shape, and partially protected entrance due to the Cíes Islands, may favour the distribution and retention of nutrients within the estuary, although synoptic comparisons of water

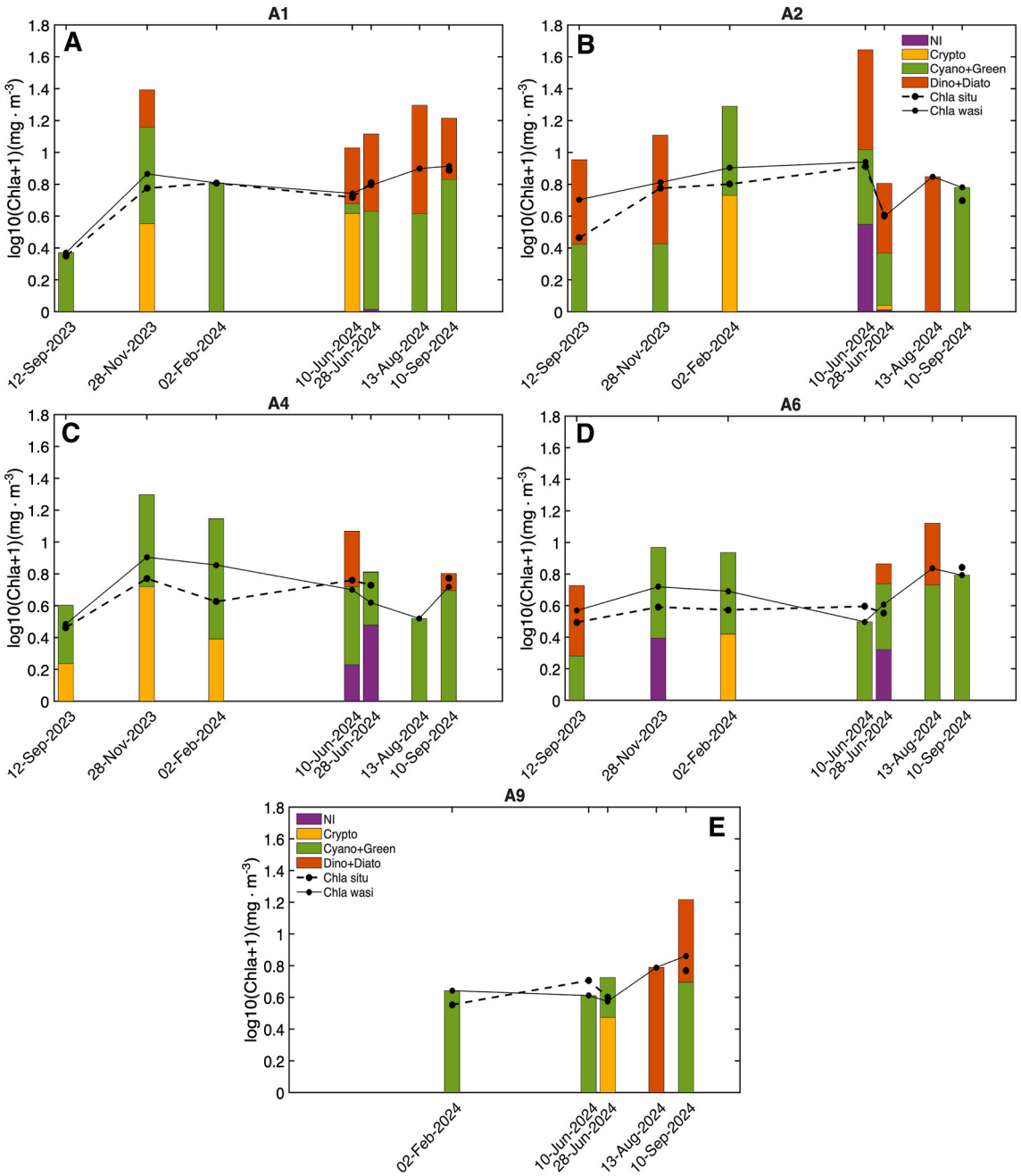

Fig. 6. Seasonal variability of phytoplankton composition with the corresponding Chl-a (C_i) derived by WASI (Non-identified phytoplankton (NI), Cryptophytes (Crypto), Cyanobacteria grouped with Green algae (Cyano + Green), Dinoflagellates grouped with Diatoms (Dino + Diato)), and total Chl-a estimated by WASI (Chla wasi) and measured by fluorimetry (Chla situ) in Ría de Arousa in stations A1 (A), A2 (B), A4 (C), A6 (D), and A9 (E). Stacked bars represent the $\log_{10}(x+1)$-transformed contribution of different phytoplankton groups. The dashed and solid lines indicate the $\log_{10}(x+1)$-transformed total Chl-a in-situ and Chl-a WASI ($mg \cdot m^{-3}$), respectively, at each sampling date. (For interpretation of the references to colour in this figure legend, the reader is referred to the Web version of this article.)

renewal times with Ría de Arousa have not been performed (Prego and Fraga, 1992; Álvarez-Salgado et al., 2000).

The application of WASI inversion (2D module; Gege, 2014) to satellite data illustrates its potential for extending this study to synoptic scales (Fig. S1). Spatial patterns retrieved from Sentinel-2 imagery acquired during an in-situ survey in Ría de Vigo suggest that the northern sections of the estuaries are predominantly influenced by dinoflagellates, whereas the southern areas have higher concentrations of non-algal particles (NAP), associated with inorganic sediments and detritus. However, the validation of these satellite-derived estimates against in-situ measurements was not possible due to the limited availability of cloud-free imagery coinciding with sampling dates and the small number of concurrent in-situ stations (n = 3). Moreover, CDOM contributions were more pronounced in the Arousa and Vigo estuaries, with the lowest levels observed in Ría de Pontevedra. Once the dominant optical constituent is identified as microplankton, it becomes possible to apply species-specific detection indices, such as the empirical reflectance-based method (AMI) (McGlinchey et al., 2025) and hyperspectral pigment-specific line height algorithms using hyperspectral satellite missions (Zoffoli et al., 2026), targeted at harmful taxa. Integrating this complementary technique could help to reduce misinterpretations, such as false positives, and enable the tracking of

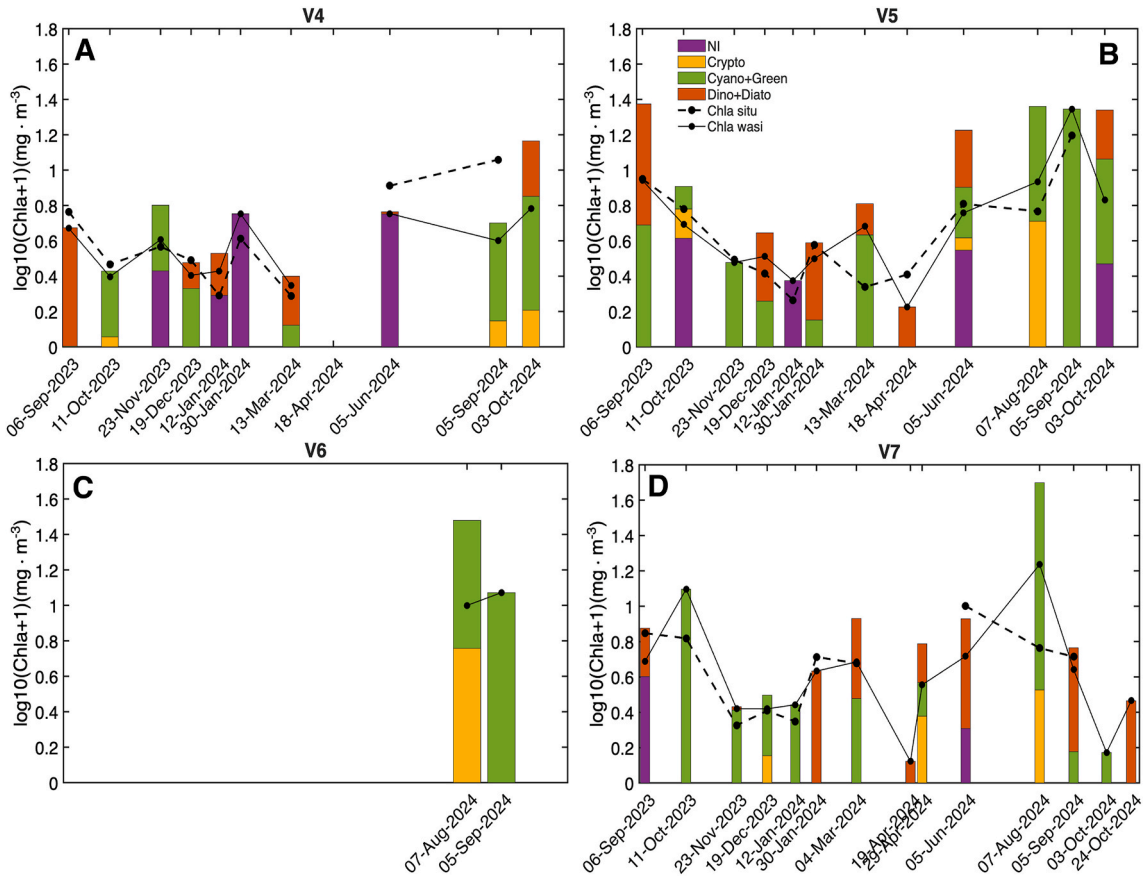

Fig. 7. Seasonal variability of phytoplankton composition with the corresponding Chl-a (C_i) derived by WASI (Non-identified phytoplankton (NI), Cryptophytes (Crypto), Cyanobacteria plus Green algae (Cyano + Green), Dinoflagellates plus Diatoms (Dino + Diato)), and total Chl-a estimated by WASI (Chla wasi) and measured by fluorimetry (Chla situ) in Ría de Vigo in stations V4 (A), V5 (B), V6 (C), and V7 (D). Stacked bars represent the $\log_{10}(x+1)$-transformed contribution of different phytoplankton groups. The dashed and solid lines indicate the $\log_{10}(x+1)$-transformed total Chl-a in-situ and Chl-a WASI ($mg{\cdot}m^{-3}$), respectively, at each sampling date. (For interpretation of the references to colour in this figure legend, the reader is referred to the Web version of this article.)

high-concentration blooms, which can inform mitigation strategies aimed at minimizing impacts on the shellfish industry in the Rías Baixas. Thereby, these findings highlight the potential of WASI as a promising tool for assessing the spatial and temporal distribution of in-water optical constituents, including the discrimination of phytoplankton groups, particularly for larger phytoplankton cells (>20 μm), while providing a cost-effective and time-efficient alternative to traditional methods. Many of the toxin-producing phytoplankton species that occur in the Rías Baixas are from microplankton groups, for which WASI may provide synoptic information at near-real time, when applied to satellite imagery. However, further validation using in-situ datasets is required to assess the uncertainties associated with satellite-based application of the WASI inversion for different sensors (Gege, 1998; Albert and Mobley, 2003). Future developments could enable WASI to discriminate between phytoplankton types, enhancing its capacity for more specific ecological monitoring.

In summary, our findings suggest that during summer, Ría de Vigo exhibited homogeneous surface SST and deeper MLD (at least at the stations and dates sampled in this study; Fig. 2), creating conditions favourable for phytoplankton blooms especially of larger groups, and potentially increasing the risk of HABs. In contrast, Ría de Arousa displayed greater variability in SST and shallower MLDs, reflecting a more dynamic environment that supports water circulation and renewal, preventing the dominance of single phytoplankton groups. The differences in optical and ecological properties between Ría de Arousa and Ría de Vigo have significant implications for aquaculture and ecosystem management. Ría de Arousa, which hosts approximately 68.5% of all mussel rafts in Galicia, benefits from its extensive open waters and optimal environmental conditions for aquaculture production. On the other hand, Ría de Vigo remains an important aquaculture area but is more susceptible to nutrient retention and associated risks, such as HAB events (Detoni et al., 2024). Understanding these dynamics is therefore critical for the sustainable management of these estuaries and the mitigation of ecological risks. In the present study, the WASI inversion approach applied to in-situ $R_{rs}(\lambda)$ demonstrated its potential as a valuable tool for monitoring estuarine systems. By accurately estimating Chl-a and characterizing the seasonal and spatial variability of a complete suite of ocean-colour properties, this approach provides a cost-effective and efficient method for tracking ecological processes, including phytoplankton diversity and bloom dynamics, in these highly productive systems. Further studies should, however, evaluate the uncertainty of the IOPs and of all phytoplankton groups, which were not addressed herein.

Overall, the WASI inversion approach provides a useful framework for linking bio-optical properties with phytoplankton dynamics in optically complex coastal environments. However, while the method shows good performance in estimating Chl-a and resolving broad phytoplankton groups, its reliance on predefined optical classes and absorption spectra that do not fully represent the local phytoplankton assemblages introduces uncertainties that should be considered. Despite these limitations, the approach provides valuable insights into spatio-temporal variability and represents a useful tool for environmental monitoring in coastal systems. Furthermore, the integration of WASI-derived products with satellite ocean-colour observations offers promising potential for scaling these analyses to broader spatial and temporal domains, supporting improved monitoring of coastal ecosystems.

The contrasting ecological features of the Ría de Arousa and Ría de Vigo highlight the importance of accounting for estuary-specific hydrodynamic and anthropogenic conditions when interpreting phytoplankton dynamics. Ría de Arousa, despite hosting the largest number of mussel rafts, tends to sustain year-round dominance of small flagellates under persistently shallower mixed layers. In contrast, Ría de Vigo, with fewer mussel rafts but deeper summer mixed layers and stronger upwelling influence, favours the development of larger phytoplankton blooms and appears more vulnerable to nutrient retention and HAB events. These differences emphasize the need for tailored monitoring and management strategies across the Rías Baixas. Future research should focus on improving local parameterisation, expanding validation datasets and integrating inversion of satellite observations and biogeochemical modelling to improve the understanding of estuarine dynamics and to support the sustainable development of aquaculture in these highly productive coastal ecosystems.

5. Conclusions

This study represents the first attempt to demonstrate the potential and utility of WASI for analysing phytoplankton diversity and the variability of optical constituents in two large embayments of the NW Iberian upwelling system, Ría de Arousa and Ría de Vigo. Despite some limitations, including the absence of in-situ IOP measurements and full taxonomic phytoplankton data coverage across all size classes for validation, the results contribute to advancing the understanding of bio-optical variability and phytoplankton dynamics in these optically complex estuarine waters.

One of the most relevant contributions of this study is the ability of WASI to differentiate phytoplankton from other dominant optical constituents, such as CDOM and detritus. However, the limited taxonomic resolution of the method constrains its capacity to resolve the full structure of the phytoplankton community, particularly for pico- and nanoplankton. This limitation is particularly important in the Rías Baixas, where smaller phytoplankton groups play a key role in microbial plankton dynamics and respond rapidly to short-term hydrographic variability (Froján et al., 2014, 2025; Hernández-Ruiz et al., 2018). These groups can alternate in dominance with microplankton depending on upwelling-downwelling cycles, nutrient availability, and biological interactions, processes that are only partially captured in the present analysis.

Our findings suggest that phytoplankton represents the dominant OAC in both estuaries throughout the year, despite the influence of continental drainage and aquaculture activities, which may enhance detritus accumulation (at least in the deeper layers). Distinct differences were observed between the two systems: Ría de Arousa exhibited higher phytoplankton diversity with co-dominance of small flagellates alongside other groups (micro-in summer and pico-in winter), likely linked to stronger exchange with oceanic waters and shallower MLDs, whereas Ría de Vigo showed conditions more favourable for blooms of larger cells, associated with deeper summer MLDs and more homogeneous surface conditions, potentially increasing the risk of HABs.

This study also highlights the potential of inversion-based approaches for supporting the development of satellite applications in optically complex coastal environments. Future improvements should focus on expanding in-situ datasets, refining optical parameterisation, and enhancing taxonomic resolution. The integration of hyperspectral radiometry with current and future hyperspectral satellite missions (*e.g.*, PRISMA, EnMAP, or CHIME) will provide improved spectral capabilities for detecting pigment-specific signals and resolving phytoplankton diversity. Ultimately, these advances will strengthen the capacity to monitor phytoplankton dynamics across size classes, from micro-to picoplankton, and to better support the management of productive and vulnerable coastal ecosystems such as the Rías Baixas.

Declaration of generative AI and AI-assisted technologies in the manuscript revision

During the revision of this manuscript, the author(s) used Claude (Anthropic) to review English grammar and style. After using this tool, the author(s) reviewed and edited the content as needed and take(s) full responsibility for the content of the published article.

CRediT authorship contribution statement

Amália Maria Sacilotto Detoni: Conceptualization, Data curation, Formal analysis, Investigation, Methodology, Validation, Visualization, Writing – original draft, Writing – review & editing. **Natalia Rudorff Oliveira:** Conceptualization, Data curation, Formal analysis, Investigation, Methodology, Visualization, Writing – original draft, Writing – review & editing. **Maria Laura Zoffoli:** Conceptualization, Data curation, Formal analysis, Investigation, Supervision, Visualization, Writing – original draft, Writing – review & editing. **Peter Gege:** Data curation, Formal analysis, Software, Validation, Writing – original draft, Writing – review & editing. **Isabel Caballero:** Formal analysis, Visualization, Writing – original draft, Writing – review & editing. **Gabriel Navarro:** Formal analysis, Funding acquisition, Supervision, Visualization. **Marcos Fontela:** Formal analysis. **María Jesús Álvarez Fernandéz:** Formal analysis. **María López Serrano:** Formal analysis. **Laura Moreno:** Formal analysis. **Isabel Gomes Teixeira:** Formal analysis. **Antón Velo:** Formal analysis, Project administration. **Xosé Antonio Padín:** Formal analysis, Funding acquisition, Investigation, Methodology, Project administration, Resources, Supervision, Visualization, Writing – original draft, Writing – review & editing.

Declaration of competing interest

The authors declare that they have no known competing financial interests or personal relationships that could have appeared to influence the work reported in this paper.

Acknowledgments

This research has been financially supported by the Grant CNS2023-143630 funded by MICIU/AEI/10.13039/501100011033 and by European Union Next Generation EU/PRTR. This work represents a contribution to the CSIC Thematic Interdisciplinary Platforms PTI TELEDETECT and PTI OCEANS+. Additionally, this work was funded by the project "ERDF A way of making Europe", the OAPN (Observatorio TIAMAT, REF: 2715/2021). The fieldwork and A.M.S.D. were supported by REDEIRA (TED2021-132188B-I00) project, funded by MCIN/AEI/10.13039/501100011033. We thank Jianwei Wei for kindly providing the Optical Water Types classification code. Thanks to José Luis Garrido from IIM-CSIC for allowing us to include in this work the HPLC measurements of phytoplankton samples from the Ría de Vigo. L.M. was supported by FCT - Fundação para a Ciência e Tecnologia, I.P. by project reference and DOI identifier https://doi.org/10.54499/PRT/BD/154754/2023.

Appendix A. Supplementary data

Supplementary data to this article can be found online at https://doi.org/10.1016/j.ecss.2026.109976.

Data availability

Data will be made available on request.

References

Albert, A., 2004. Inversion Technique for Optical Remote Sensing in Shallow Water. Universität Hamburg, Hamburg, Germany, p. 188. Ph.D. Dissertation.

Albert, A., Mobley, C.D., 2003. An analytical model for subsurface irradiance and remote sensing reflectance in deep and shallow case-2 waters. Opt. Express 11, 2873–2890. https://doi.org/10.1364/oe.11.002873.

Barton, E.D., Largier, J.L., Torres, R., Sheridan, M., Trasviña, A., Souza, A., Pazos, Y., Valle-Levinson, A., 2015. Coastal upwelling and downwelling forcing of circulation in a semi-enclosed bay: ria de Vigo. Prog. Oceanogr. 134, 173–189. https://doi.org/10.1016/j.pocean.2015.01.014.

Bi, S., Hieronymi, M., Röttgers, R., 2023. Bio-geo-optical modelling of natural waters. Front. Mar. Sci. 10. https://doi.org/10.3389/fmars.2023.1196352.

Bilbao, J., Seoane, S., 2024. PIGMENTUM: an easy pigment-based tool for monitoring phytoplankton community composition. Mar. Ecol. Prog. Ser. 729, 31–45. https://doi.org/10.3354/meps14518.

Detoni, A.M.S., Navarro, G., Padín, X.A., Ramirez-Romero, E., Zoffoli, M.L., Pazos, Y., Caballero, I., 2024. Potentially toxigenic phytoplankton patterns in the northwestern Iberian Peninsula. Front. Mar. Sci. 11. https://doi.org/10.3389/fmars.2024.1330090.

Figueiras, F.G., Teixeira, I.G., Froján, M., Zúñiga, D., Arbones, B., Castro, C.G., 2020. Seasonal variability in the microbial Plankton community in a semienclosed Bay affected by upwelling: the role of a nutrient trap. Front. Mar. Sci. 7, 578042. https://doi.org/10.3389/fmars.2020.578042.

Figueiras, F.G., Pazos, Y., 1991. Microplankton assemblages in three Rías Baixas (Vigo, Arosa and Muros, Spain) with a subsurface chlorophyll maximum: their relationships to hydrography. Mar. Ecol. Prog. Ser. 76 (3), 219–233. https://doi.org/10.3354/MEPS076219.

Froján, M., Arbones, B., Zúñiga, D., Castro, C.G., Figueiras, F.G., 2014. Microbial plankton community in the Ría de Vigo (NW Iberian upwelling system): impact of the culture of *Mytilus galloprovincialis*. Mar. Ecol. Prog. Ser. 498, 43–54. https://doi.org/10.3354/meps10612.

Froján, M., Muñoz-Colmenero, M., Teixeira, I.G., Arbones, B., Sotelo, C.G., Correa, B., Figueiras, F.G., Castro, C.G., 2025. Unveiling short-scale responses: how Pico- and nanoeukaryotic plankton navigate environmental variability in a coastal upwelling System. Environ. Microbiol. Rep. 17, e70070. https://doi.org/10.1111/1758-2229.70070.

Gege, P., 1998. Characterization of the phytoplankton in Lake Constance for classification by remote sensing. In: Bäuerle, E., Gaedke, U. (Eds.), Lake Constance—Characterisation of an Ecosystem in Transition, vol. 53. Archiv für Hydrobiologie, pp. 179–193.

Gege, P., 2004. The water colour simulator WASI: an integrating software tool for analysis and simulation of optical in situ spectra. Comput. Geosci. 30, 523–532. https://doi.org/10.1016/j.cageo.2004.03.005.

Gege, P., 2014. WASI-2D: a software tool for regionally optimized analysis of imaging spectrometer data from deep and shallow waters. Comput. Geosci. 62, 208–215. https://doi.org/10.1016/j.cageo.2013.07.022.

Gege, P., Albert, A., 2006. A tool for inverse modeling of spectral measurements in deep and shallow waters. In: Richardson, L.L., LeDrew, E.F. (Eds.), Remote Sensing of Aquatic Coastal Ecosystem Processes: Science and Management Applications", Kluwer Book Series: Remote Sensing and Digital Image Processing. Springer, pp. 81–109. ISBN 1-4020-3967-0.

Glover, D.M., Brewer, P.G., 1988. Estimates of wintertime mixed layer nutrient concentrations in the North Atlantic. Deep-Sea Res. Part A Oceanogr. Res. Pap. 35 (9), 1525–1546. https://doi.org/10.1016/0198-0149(88)90101-X.

Hernández-Ruiz, M., Barber-Lluch, E., Prieto, A., Álvarez-Salgado, X.A., Logares, R., Teira, E., 2018. Seasonal succession of small planktonic eukaryotes inhabiting surface waters of a coastal upwelling system. Environ. Microbiol. 20, 2955–2973. https://doi.org/10.1111/1462-2920.14313.

Hillebrand, H., Dürselen, C., Kirschtel, D., Pollingher, U., Zohary, T., 1999. Biovolume calculation for pelagic and benthic microalgae. J. Phycol. 35, 403–424. https://doi.org/10.1046/j.1529-8817.1999.3520403.x.

IOCCG, 2006. Remote sensing of inherent optical properties: fundamentals, tests of algorithms, and applications. Lee, ZhongPing. Reports of the International Ocean-Colour Coordinating Group, Number 5. IOCCG, Dartmouth, NS, Canada.

Kara, A.B., Rochford, P.A., Hurlburt, H.E., 2000. An optimal definition for ocean mixed layer depth. J. Geophys. Res. Oceans 105 (C7), 16803–16821. https://doi.org/10.1029/2000JC900072.

Lee, Z.P., 2014. Update of the Quase-Analytical algorithm. QAA_v6). http://www.ioccg.org/groups/Software_OCA/QAA_v6_202011.pdf.

Lee, Z.P., et al., 2002. Deriving inherent optical properties from water colour: a multiband quasi-analytical algorithm for optically deep waters. Appl. Opt. 41 (27), 5755–5772. https://doi.org/10.1364/AO.41.005755.

Álvarez-Salgado, X.A., Gago, J., Míguez, B.M., Gilcoto, M., Pérez, F.F., 2000. Surface waters of the NW Iberian margin: upwelling on the shelf versus outwelling of upwelled waters from the Rías Baixas. Estuar. Coast Shelf Sci. 51 (6), 821–837. https://doi.org/10.1006/ecss.2000.0714.

Álvarez-Salgado, X.A., Labarta, U., Fernández-Reiriz, M.J., Figueiras, F.G., Rosón, G., Piedracoba, S., Filgueira, R., Cabanas, J.M., 2008. Renewal time and the impact of harmful algal blooms on the extensive mussel raft culture of the Iberian coastal upwelling system (SW Europe). Harmful Algae 7, 849–855. https://doi.org/10.1016/J.HAL.2008.04.007.

Maire, L., Gege, P., Damm, A., Odermatt, D., 2025. Differentiating phytoplankton taxa in lakes using hyperspectral *in situ* reflectance and imaging microscopy. Sci. Total Environ. 1003, 180718. https://doi.org/10.1016/j.scitotenv.2025.180718.

Marañón, E., 2015. Cell size as a key determinant of phytoplankton metabolism and community structure. Ann. Rev. Mar. Sci 7, 241–264. https://doi.org/10.1146/annurev-marine-010814-015955.

Maritorena, S., Siegel, D.A., Peterson, A.R., 2002. Optimization of a semianalytical ocean color model for global-scale applications. Appl. Opt. 41 (15), 2705–2714. https://doi.org/10.1364/AO.41.002705.

McGlinchey, C., Torres Palenzuela, J., Gonzalez-Vilas, L., Werther, M., Jiang, D., Tyler, A., Pazos, Y., Spyrakos, E., 2025. Optical properties of a toxin-producing dinoflagellate and its detection from Sentinel-2 MSI in nearshore waters. ISPRS J. Photogrammetry Remote Sens. 227, 415–437. https://doi.org/10.1016/j.isprsjprs.2025.06.017.

Menden-Deuer, S., Lessard, E.J., 2000. Carbon to volume relationships for dinoflagellates, diatoms, and other protist plankton. Limnol. Oceanogr. 45, 569–579. https://doi.org/10.4319/lo.2000.45.3.0569.

Morel, A., Antoine, D., 1994. Heating rate within the upper ocean in relation to its bio–optical state. J. Phys. Oceanogr. 24, 1652–1665, 0.1175/1520-0485(1994)024<1652:HRWTUO>2.0.CO;2.

Nelder, J.A., Mead, R., 1965. A simplex method for function minimization. Comput. J. 7, 308–313. https://doi.org/10.1093/comjnl/7.4.308.

Neveux, J., Panouse, M., 1987. Spectrofluorometric determination, of chlorophylls and pheophytins. Arch. Hydrobiol. 109, 567–581.

Niroumand-Jadidi, M., Bovolo, F., Bruzzone, L., Gege, P., 2021. Inter-comparison of methods for chlorophyll-a retrieval: sentinel-2 time-series analysis in Italian lakes. Remote Sens. 13, 2381. https://doi.org/10.3390/rs13122381.

Nogueira, E., Bravo, I., Montero, P., Díaz-Tapia, P., Calvo, S., Ben-Gigirey, B., Figueroa, R.I., Garrido, J.L., Ramilo, I., Lluch, N., Rossignoli, A.E., Riobó, P., Rodríguez, F., 2022. HABs in coastal upwelling systems: insights from an exceptional red tide of the toxigenic dinoflagellate *Alexandrium minutum*. Ecol. Indic. 137, 108790. https://doi.org/10.1016/j.ecolind.2022.108790.

O'Reilly, J.E., Werdell, P.J., 2019. Chlorophyll algorithms for ocean color sensors – OC4, OC5 & OC6. Remote Sens. Environ. 229, 32–47. https://doi.org/10.1016/j.rse.2019.04.021.

Pardo, P.C., Bastero, S.F., Moreno, L., Castro, C.G., 2022. Implementation of a portable module for assessing the eutrophication risk: initial evaluation in the upwelling-driven bay of Ría de Arousa (NW-Iberian Peninsula). Ocean Coast. Res. 70. https://doi.org/10.1590/2675-2824070.21093PCP.

Pardo, P.C., Padín, X.A., Gilcoto, M., Farina-Busto, L., Pérez, F.F., 2011. Evolution of upwelling systems coupled to the long-term variability in sea surface temperature and Ekman transport. Clim. Res. 48 (2–3), 231–246. https://doi.org/10.3354/cr00989.

Prego, R., Fraga, F., 1992. A simple model to calculate the residual flows in a Spanish ria. Hydrographic consequences in the ria of Vigo. Estuar. Coast Shelf Sci. 34 (6), 603–615. https://doi.org/10.1016/S0272-7714(05)80065-4.

Rodríguez, F., Escalera, L., Reguera, B., Nogueira, E., Bode, A., Ruiz-Villarreal, M., et al., 2024. Red tides in the Galician rías: historical overview, ecological impact, and future monitoring strategies. Environ. Sci. Process. Impacts 26, 16–34. https://doi.org/10.1039/d3em00296a.

Rosón, G., Álvarez-Salgado, X.A., Pérez, F.F., 1997. A non-stationary box-model to determine residual flows in a partially mixed estuary, based on both thermohaline properties. Application to the Ría de Arousa (NW Spain). Estuar. Coast Shelf Sci. 44, 249–262. https://doi.org/10.1006/ecss.1996.0127.

Rosón, G., Pérez, F.F., Álvarez-Salgado, X.A., Figueiras, F.C., 1995. Variation of both thermohaline and chemical properties in an estuarine upwelling ecosystem: Ría de Arousa. I. Temporal evolution. Estuar. Coast Shelf Sci. 41, 195–213. https://doi.org/10.1006/ecss.1995.0061.

Sathyendranath, S., Stuart, V., Nair, A., Oka, K., Nakane, T., Bouman, H., Forget, M.-H., Maass, H., Platt, T., 2009. Carbon-to-chlorophyll ratio and growth rate of phytoplankton in the sea. Mar. Ecol. Prog. Ser. 383, 73–84. https://doi.org/10.3354/meps07998.

Smith, R., Baker, K., 1986. Analysis of ocean optical data. In: Slater, P.N. (Ed.), *Ocean Optics.*, VIII. SPIE, 637: 95–637: 107.

Sun, X., Brewin, R.J.W., Sathyendranath, S., Dall'Olmo, G., Antoine, D., Barlow, R., Bracher, A., Kheireddine, M., Li, M., Raitsos, D.E., Shen, F., Tilstone, G.H., Vellucci, V., 2025. Coupling ecological concepts with an ocean-colour model: parameterisation and forward modelling. Remote Sens. Environ. 316, 114487. https://doi.org/10.1016/j.rse.2024.114487.

Tilstone, G.H., Figueiras, F.G., Fraga, F., 1994. Upwelling-downwelling sequences in the generation of red tides in a coastal upwelling system. Mar. Ecol. Prog. Ser. 112 (3), 241–253.

Uitz, J., Claustre, H., Morel, A., Hooker, S.B., 2006. Vertical distribution of phytoplankton communities in open ocean: an assessment based on surface chlorophyll. J. Geophys. Res. Oceans 111 (C8). https://doi.org/10.1029/2005JC003207.

Utermöhl, H., 1958. Zur Vervollkommung der quantitativen Phytoplankton Methodik. Mitt. Int. Ver. Limnol. 9, 1–38.

Wei, J., Wang, M., Mikelsons, K., Jiang, L., Kratzer, S., Lee, Z., Moore, T., Sosik, H.M., Van der Zande, D., 2022. Global satellite water classification data products over oceanic, coastal, and inland waters. Remote Sens. Environ. 282, 113233. https://doi.org/10.1016/j.rse.2022.113233.

Werdell, P.J., Roesler, C.S., Goes, J.I., 2014. Discrimination of phytoplankton functional groups using an ocean reflectance inversion model. Appl. Opt. 53, 4833. https://doi.org/10.1364/ao.53.004833.

Xi, H., Hieronymi, M., Krasemann, H., Röttgers, R., 2017. Phytoplankton group identification using simulated and in situ hyperspectral remote sensing reflectance. Front. Mar. Sci. 4. https://doi.org/10.3389/fmars.2017.00272.

Zapata, M., Rodríguez, F., Garrido, J.L., 2000. Separation of chlorophylls and carotenoids from marine phytoplankton: a new HPLC method using a reversed phase of C8 column and pyridine-containing mobile phases. Mar. Ecol. Prog. Ser. 195, 29–45. https://doi.org/10.3354/meps195029.

Zibordi, G., Voss, K.J., Johnson, B.C., Mueller, J.L., 2019. Protocols for satellite ocean colour data validation: in situ optical radiometry. IOCCG Ocean Optics and Biogeochemistry Protocols for Satellite Ocean Colour Sensor Validation 3 (0). https://doi.org/10.25607/OBP-691.

Zoffoli, M.L., Pochic, V., Bresciani, M., Braga, F., Lacour, T., Retho, M., Manach, S., Röttgers, R., Detoni, A.M.S., Harmel, T., Gernez, P., 2026. Toward elucidation of Harmful Algal bloom (HAB) dominant-class using hyperspectral satellite remote sensing. Remote Sens. Environ. 341, 115439. https://doi.org/10.1016/j.rse.2026.115439.